OPEN ACCESS

GAVIN PUBLISHERS

International Journal of Pollution Research

Alkhidir KEME. J Pollut Res: IJPR-104.

DOI: 10.29011/IJPR -104.000004

Review Article

Seismo Electric Bio availability Fractal Dimension for Characterizing Shajara Reservoirs of the Permo-Carboniferous Shajara Formation, Saudi Arabia

Khalid Elyas Mohamed Elameen Alkhidir*

Department of Petroleum and Natural Gas Engineering, College of Engineering, King Saud University, Riyadh, Saudi Arabia

***Corresponding author:** Khalid Elyas Mohamed Elameen Alkhidir, Department of Petroleum and Natural Gas Engineering, College of Engineering, King Saud University, Riyadh, Saudi Arabia. Tel: +966114679118; Email: kalkhidir@ksu.edu.sa

Citation: Alkhidir KEME (2018) Seismo Electric Bio Availability Fractal Dimension for Characterizing Shajara Reservoirs of the Permo -Carboniferous Shajara Formation, Saudi Arabia.Int J Pollut Res: IJPR-104. DOI: 10.29011/IJPR -104.000004

Received Date: 16 September, 2018; **Accepted Date:** 01 October, 2018; **Published Date:** 09 October, 2018

Abstract

The quality and assessment of a reservoir can be documented in details by the application of Seismo Electric Bio availability. This research aims to calculate fractal dimension from the relationship among seismo electric bioavailability, maximum seismo electric bioavailability and wetting phase saturation and to approve it by the fractal dimension derived from the relationship among capillary pressure and wetting phase saturation. In this research, porosity was measured on real collected sandstone samples and permeability was calculated theoretically from capillary pressure profile measured by mercury intrusion contaminating the pores of sandstone samples in consideration. Two equations for calculating the fractal dimensions have been employed. The first one describes the functional relationship between wetting phase saturation, seismo electric bioavailability, maximum Seismo Electric Bioavailability and Fractal Dimension. The second equation implies to the wetting phase saturation as a function of capillary pressure and the fractal dimension. Two procedures for obtaining the fractal dimension have been utilized. The first procedure was done by plotting the logarithm of the ratio between seismo electric bio availability and maximum seismo electric bio availability versus logarithm wetting phase saturation. The slope of the first procedure = 3- Df (fractal dimension). The second procedure for obtaining the fractal dimension was determined by plotting the logarithm of capillary pressure versus the logarithm of wetting phase saturation. The slope of the second procedure = Df -3. On the basis of the obtained results of the fabricated stratigraphic column and the attained values of the fractal dimension, the sandstones of the Shajara reservoirs of the Shajara Formation were divided here into three units. The obtained units from bottom to top are: Lower, Middle and Upper Shajara Seismo Electric Bio Availability Fractal Dimension Units. It was found that fractal dimension increases with increasing grain size and permeability

Keywords: Seismo Electric Bioavailability; Shajara Formation; Shajara Reservoirs

Introduction

Seismo electric effects related to electro kinetic potential, dielectric permittivity, pressure gradient, fluid viscosity, and electric conductivity was first reported by [1]. Capillary pressure follows the scaling law at low wetting phase saturation was reported by [2]. Seismo electric phenomenon by considering electro kinetic coupling coefficient as a function of effective charge density, permeability, fluid viscosity and electric conductivity was reported by [3]. The magnitude of seismo electric current depends porosity, pore size, zeta potential of the pore surfaces, and elastic properties of the matrix was investigated by [4]. The tangent of the ratio of converted electric field to pressure is approximately in inverse proportion to permeability was studied by [5]. Permeability inversion from seismoelectric log at low frequency was studied by [6]. They reported that, the tangent of the ratio among electric excitation intensity and pressure field is a function of porosity, fluid viscosity, frequency, tortuosity, fluid density and Dracy permeability. A decrease of seismo electric frequencies with increasing water content was reportet by [7]. An increase of seismo electric transfer function with increasing water saturation was studied by [8]. An increase of dynamic seismo electric transfer function with decreasing fluid conductivity was described by [9]. The amplitude of seismo electric signal increases with increasing permeability which means that the seismo electric effects are directly related to the permeability and can be used to

study the permeability of the reservoir was illustrated by [10]. Seismo electric coupling is frequency dependent and decreases exponentially when frequency increases were demonstrated by [11]. An increase of permeability with increasing pressure head and bubble pressure fractal dimension was reported by [12,13]. An increase of geometric and arithmetic relaxation time of induced polarization fractal dimension with permeability increasing was described by [14,15].

Material and Method

Sandstone samples were collected from the surface type section of the Permo-Carboniferous Shajara Formation, latitude 26 52 17.4, longitude 43 36 18. (Figure1). Porosity was measured on collected samples using mercury intrusion Porosimetry and permeability was derived from capillary pressure data. The purpose of this paper is to obtain seismo electric bio availability fractal dimension and to confirm it by capillary pressure fractal dimension. The fractal dimension of the first procedure is determined from the positive slope of the plot of logarithm of the ratio of seismo electric bio availability to maximum seismo electric bio availability log ($SEBA^{1/2}$ /$SEBA_{max}^{1/2}$) versus log wetting phase saturation (log Sw). Whereas the fractal dimension of the second procedure is determined from the negative slope of the plot of logarithm of log capillary pressure (log Pc) versus logarithm of wetting phase saturation (log Sw).

The seismo electric bio availability can be scaled as

$$W = \left[\frac{SEBA^{\frac{1}{2}}}{SEBA_{max}^{\frac{1}{2}}}\right]^{|3-Df|} \quad (1)$$

Where Sw the water saturation, SEBA seismo electric bio availability in kilo gram * second / liter, $SEBA_{max}$ the maximum seismo electric bio availability in kilo gram *second / liter, and Df the fractal dimension

Equation 1 can be proofed from

$$J = \sigma * E \quad (2)$$

Where J the electric current density in ampere /square meter, σ the electric conductivity in Siemens /meter, and E the seismo electric field in volt /meter.

The electric conductivity can be scaled as

$$\sigma = \left[\frac{reff^2 * C_E}{8 * \eta * C_S}\right] \quad (3)$$

Where σ the electric conductivity in Siemens / meter, reff the effective pore size in mete, C_E the electro osmosis coefficient in pascal /volt, η the fluid viscosity in pascal*second, C_S the streaming potential coefficient in volt / pascal.

Insert equation 3 into equation 2

$$J = \left[\frac{reff^2 * C_E * E}{8 * \eta * C_S}\right] \quad (4)$$

The viscosity can be scaled as

$$\eta = P * t \quad (5)$$

Where η the fluid viscosity in pascal*second, p the pressure in pascal, and the time in second.

Insert equation 5 into equation 4

$$J = \left[\frac{reff^2 * C_E * E}{8 * P * t * C_S}\right] \quad (6)$$

The pressure can be scaled as

$$P = \left[\frac{F}{A}\right] \quad (7)$$

Where P the pressure in pascal, F the force in newton, and the area in square meter.

Insert equation 7 into equation 6

$$J = \left[\frac{reff^2 * C_E * E * A}{8 * F * t * C_S}\right] \quad (8)$$

The force can be scaled as

$$F = m * g \quad (9)$$

Where F the force in newton, m the mass in kilo gram, and g the acceleration in meter /square second.

Insert equation 9 into equation 8

$$J = \left[\frac{reff^2 * C_E * E * A}{8 * m * g * t * C_S}\right] \quad (10)$$

The mass can be scaled as

$$m = \rho * V \quad (11)$$

Where m the mass in kilo gram, ρ the density in kilo gram / cubic meter, and V the volume

Insert equation 11 into equation 10

$$J = \left[\frac{reff^2 * C_E * E * A}{8 * \rho * V * g * t * C_S}\right] \quad (12)$$

$$\text{But; } \rho * t = SEBA \quad (13)$$

Where ρ the density in kilo gram / cubic meter, t the time in second, and SEBA the seismo electric bio availability in kilo gram *second / liter.

Insert equation 13 into equation 12

$$J = \left[\frac{reff^2 * C_E * E * A}{8 * SEBA * V * g * C_S}\right] \quad 14$$

Introduce the pore size r in meter in equation 14

$$J = \left[\frac{r^2 * C_E * E * A}{8 * SEBA * V * g * C_S}\right] \quad 15$$

Equation 15 after rearrangement will become

$$SEBA = \left[\frac{r^2 * C_E * E * A}{8 * J * V * g * C_S}\right] \quad 16$$

The maximum pore radius can be scaled as

$$SEBA_{max} = \left[\frac{r_{max}^2 * C_E * E * A}{8 * J * V * g * C_S}\right] \quad 17$$

Divide equation 16 by equation 17

$$\left[\frac{SEBA}{SEBA_{max}}\right] = \left[\frac{\left[\frac{r^2 * C_E * E * A}{8 * J * V * g * C_S}\right]}{\left[\frac{r_{max}^2 * C_E * E * A}{8 * J * V * g * C_S}\right]}\right] \quad 18$$

Equation 18 after simplification will become

$$\left[\frac{SEBA}{SEBA_{max}}\right] = \left[\frac{r^2}{r_{max}^2}\right] \quad 19$$

Take the square root of equation 19

$$\sqrt{\left[\frac{SEBA}{SEBA_{max}}\right]} = \sqrt{\left[\frac{r^2}{r_{max}^2}\right]} \quad 20$$

Equation 20 after simplification will become

$$\left[\frac{SEBA^{\frac{1}{2}}}{SEBA_{max}^{\frac{1}{2}}}\right] = \left[\frac{r}{r_{max}}\right] \quad 21$$

Take the logarithm of equation 21

$$\log\left[\frac{SEBA^{\frac{1}{2}}}{SEBA_{max}^{\frac{1}{2}}}\right] = \log\left[\frac{r}{r_{max}}\right] \quad 22$$

$$\text{But; } \log\left[\frac{r}{r_{max}}\right] = \frac{\log Sw}{[3 - Df]} \quad 23$$

Insert equation 23 into equation 22

$$\frac{\log Sw}{[3 - Df]} = \log\left[\frac{SEBA^{\frac{1}{2}}}{SEBA_{max}^{\frac{1}{2}}}\right] \quad 24$$

Equation 24 after log removal will become

$$Sw = \left[\frac{SEBA^{\frac{1}{2}}}{SEBA_{max}^{\frac{1}{2}}}\right]^{[3-Df]} \quad 25$$

Equation 25 the proof of equation 1 which relates the water saturation, the seismo electric bio availability, maximum seismo electric bio availability, and the fractal dimension.

The capillary pressure can be scaled as

$$Sw = \left[\frac{F^{\frac{1}{3}}}{F_{max}^{\frac{1}{3}}}\right]^{[3-Df]} \quad 26$$

Where Sw, the water saturation, F the seismo mechanical force in Newton, F_{max}, the maximum seismo mechanical force in Newton and Df the fractal dimension.

Equation 26 can be proofed from electric current density taking into account the electro kinetic effect, angular frequency, seismic displacement and fluid density.

$$J = C_{EK} * \omega^2 * U_s * \rho_f \quad 27$$

Where J the electric current density in ampere / square meter, C_{EK} the electro kinetic coefficient in ampere / (pascal * meter), ω the seismic angular frequency in hertz, Us the seismic displacement in meter, and ρf the fluid density in kilogram / cubic meter.

$$\text{But; } \rho_f = \left[\frac{m}{V}\right] \quad 28$$

Where ρ_f the density in kilogram /cubic meter, m the mass in kilogram, and V the volume in cubic meter.

Insert equation 28 into equation 27

$$J = \left[\frac{C_{EK} * \omega^2 * U_s * m}{V}\right] \quad 29$$

The mass m can be scaled as

$$m = \left[\frac{F}{g}\right] \quad 30$$

Where F the seismo mechanical force in Newton, g the acceleration in meter / (square second).

Insert equation 30 into equation 29

$$J = \left[\frac{C_{EK} * \omega^2 * U_s * F}{V * g}\right] \quad 31$$

The volume in equation 31 can be scaled as

$$V = \left[\frac{4 * 3.14 * r^3}{3}\right] \quad 32$$

Where r the pore radius in meterInsert equation 32 into equation 31

$$J = \left[\frac{3 * C_{EK} * \omega^2 * U_s * F}{4 * 3.14 * r^3 * g}\right] \quad 33$$

The pore radius of equation 33 after rearrangement will become

$$r^3 = \left[\frac{3 * C_{EK} * \omega^2 * U_s * F}{4 * 3.14 * J * g}\right] \quad 34$$

The maximum pore radius r_{max} can be scaled as

$$r_{max}^3 = \left[\frac{3 * C_{EK} * \omega^2 * U_s * F_{max}}{4 * 3.14 * J * g}\right] \quad 35$$

Divide equation 34 by equation 35

$$\left[\frac{r^3}{r_{max}^3}\right] = \left[\frac{\left[\frac{3 * C_{EK} * \omega^2 * U_s * F}{4 * 3.14 * J * g}\right]}{\left[\frac{3 * C_{EK} * \omega^2 * U_s * F_{max}}{4 * 3.14 * J * g}\right]}\right] \quad 36$$

Equation 36 after simplification will become

$$\left[\frac{r^3}{r_{max}^3}\right] = \left[\frac{F}{F_{max}}\right] \quad 37$$

Take the third root of equation 37

$$\sqrt[3]{\left[\frac{r^3}{r_{max}^3}\right]} = \sqrt[3]{\left[\frac{F}{F_{max}}\right]} \quad 38$$

Equation 38 can also be written as

$$\left[\frac{r}{r_{max}}\right] = \left[\frac{F^{\frac{1}{3}}}{F_{max}^{\frac{1}{3}}}\right] \quad 39$$

Take the logarithm of equation 39

$$\log\left[\frac{r}{r_{max}}\right] = \log\left[\frac{F^{\frac{1}{3}}}{F_{max}^{\frac{1}{3}}}\right] \quad 40$$

$$\text{But; } \log\left[\frac{r}{r_{max}}\right] = \frac{\log Sw}{[3 - Df]} \quad 41$$

Insert equation 41 into equation 40

$$\frac{\log Sw}{[3 - Df]} = \log\left[\frac{F^{\frac{1}{3}}}{F_{max}^{\frac{1}{3}}}\right] \quad 42$$

Equation 42 after log removal will become

$$Sw = \left[\frac{F^{\frac{1}{3}}}{F_{max}^{\frac{1}{3}}}\right]^{[3-Df]} = \left[\frac{SEBA^{\frac{1}{2}}}{SEBA_{max}^{\frac{1}{2}}}\right]^{[3-Df]} \quad 43$$

Equation 43 the proof of equation 1 which relates the Water saturation, the seismo mechanical force, the maximum seismo mechanical force and the fractal dimension, seismo electric bio availability, maximum seismo electric bio availability and the fractal dimension.

The capillary pressure can be scaled as

$$\text{Log } Sw = [Df - 3] * Pc + \text{constant} \quad 44$$

Where Sw the water saturation, Pc the capillary pressure and Df the fractal dimension

Result and Discussion

Based on field observation the Shajara Reservoirs of the Shajara Formation of The Permo-Carboniferous Unayzah Group were divided here into three units as described in (Figure 1). These units from bottom to top are: Lower Shajara Reservoir, Middle Shajara reservoir, and Upper Shajara Reservoir. Their acquired results of the Seismo Electric Bioavailability Fractal Dimension and Capillary Pressure Fractal Dimension are displayed in (Table 1). Based on the attained results it was found that the Seismo Electric Bioavailability Fractal Dimension Is Equal to The Capillary Pressure Fractal Dimension. The maximum value of the fractal dimension was found to be 2.7872 assigned to sample SJ13 from the Upper Shajara Reservoir as verified in (Table 1). Whereas the minimum value of the fractal dimension 2.4379 was reported from sample SJ3 from the Lower Shajara reservoir as displayed in (Table 1). The Seismo Electric Bioavailability Fractal Dimension and Capillary Pressure Fractal Dimension were observed to increase with increasing permeability as proofed in (Table 1) owing to the possibility of having interconnected channels. The Lower Shajara reservoir was denoted by six sandstone samples (Figure 1), four of which label as SJ1, SJ2, SJ3 and SJ4 were selected for capillary pressure measurement as confirmed in (Table1). Their positive slopes of the first procedure (log of the ratio of seismo electric bioavailability to maximum seismo electric bio availability versus log wetting phase saturation) and negative slopes of the second procedure (log capillary pressure versus Log Wetting Phase Saturation (log Sw) is delineated in (Figure 2-5). Their seismo electric bio availability fractal dimension and capillary pressure fractal dimension values are shown in (Table 1). As we proceed from sample SJ2 to SJ3 a pronounced reduction in permeability due to compaction was reported from 1955 md to 56 md which reflects decrease in seismo electric bioavailability fractal dimension from 2.7748 to 2.4379 as specified in (Table 1). Again, an increase in grain size and permeability was verified from sample SJ4 whose seismo electric bio availability fractal dimension and capillary pressure fractal dimension was found to be 2.6843 as described in (Table 1). In contrast, the Middle

Shajara reservoir which is separated from the Lower Shajara reservoir by an unconformity surface as shown in (Figure 1). It was designated by four samples (Figure 1), three of which named as SJ7, SJ8, and SJ9 as illustrated in (Table1) were selected for capillary measurements as described in (Table 1). Their positive slopes of the first procedure and negative slopes ofthe second procedure are shown in (Figures 6-8). Additionally, their seismo electric bioavailability fractal dimensions and capillary pressure fractal dimensions show similarities as delineated in (Table 1). Their fractal dimensions are higher than those of samples SJ3 and SJ4 from the Lower Shajara Reservoir due to an increase in their permeability as explained in table 1. On the other hand, the Upper Shajara reservoir separated from the Middle Shajarareservoir by yellow green mudstone as revealed in (Figure 1). It is defined by three samples so called SJ11, SJ12, SJ13 as explained in (Table 1). Their positive slopes of the first procedure and negative slopes of the second procedure are displayed in (Figure 9-11).

Moreover, their seismo electric bioavailability fractal dimension and capillary pressure fractal dimension are also higher thanthose of sample SJ3 and SJ4 from the Lower Shajara Reservoir due to an increase in their permeability as clarified in (Table 1). Overall a plot of seismo electric bioavailability fractal dimension versus capillary pressure fractal dimension as shown in (Figure 12) reveals three permeable zones of varying Petrophysical properties. Such variation in fractal dimension can account for heterogeneity which is a key parameter in reservoir quality assessment. This reservoir heterogeneity was also confirmed by plotting positive slope of the first procedure versus negative slope of the second procedure as described in (Figure 13).

Formation	Reservoir	Sample	Porosity %	k(md)	Positive slope of the first procedureSlope=3-Df	Negative slope of the second procedureSlope=Df-3	Seismo electric bio availability fractal dimension	Capillary pressure fractal dimension
Permo-Carboniferous Shajara Formation	Upper Shajara Reservoir	SJ13	25	973	0.2128	-0.2128	2.7872	2.7872
		SJ12	28	1440	0.2141	-0.2141	2.7859	2.7859
		SJ11	36	1197	0.2414	-0.2414	2.7586	2.7586
	Middle Shajara Reservoir	SJ9	31	1394	0.2214	-0.2214	2.7786	2.7786
		SJ8	32	1344	0.2248	-0.2248	2.7752	2.7752
		SJ7	35	1472	0.2317	-0.2317	2.7683	2.7683
	Lower Shajara Reservoir	SJ4	30	176	0.3157	-0.3157	2.6843	2.6843
		SJ3	34	56	0.5621	-0.5621	2.4379	2.4379
		SJ2	35	1955	0.2252	-0.2252	2.7748	2.7748
		SJ1	29	1680	0.2141	-0.2141	2.7859	2.7859

Table 1: Petrophysical model showing the three Shajara Reservoir Units with their corresponding values of seismo electric bio availability fractal dimension and capillary pressure fractal dimension.

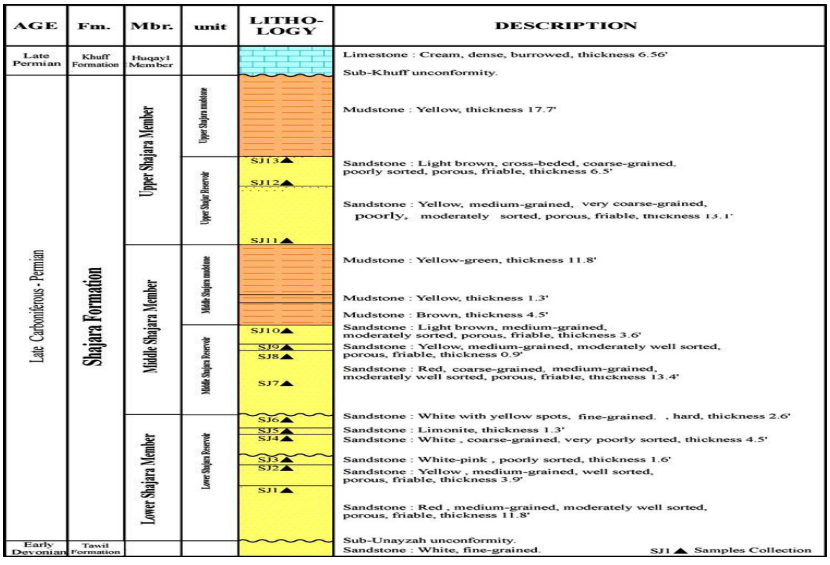

Figure 1: Surface type section of the Shajara Reservoirs of the Permo- Carboniferous Shajara Formation at latitude 26 52 17.4, longitude 43 36 18.

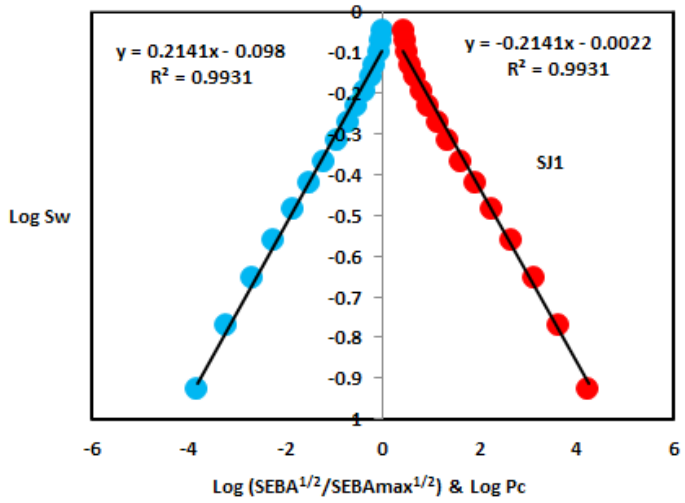

Figure 2: Log (SEBA$^{1/2}$/SEBA$_{max}^{1/2}$) & log Pc versus log Sw for sample SJ1.

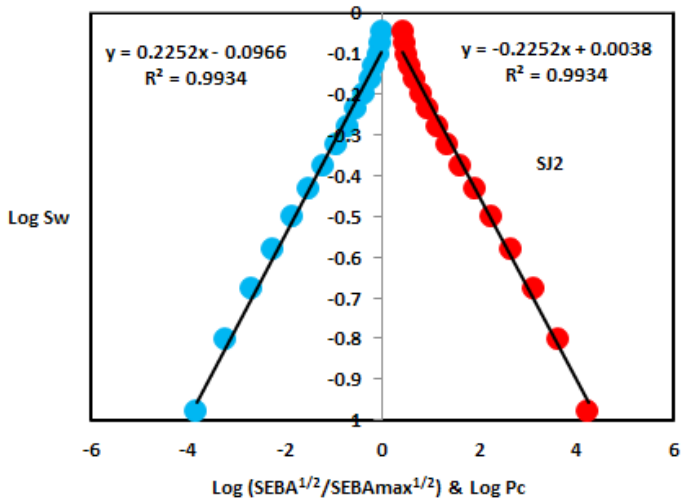

Figure 3: Log (SEBA$^{1/2}$/SEBA$_{max}^{1/2}$) & log Pc versus log Sw for sample SJ2.

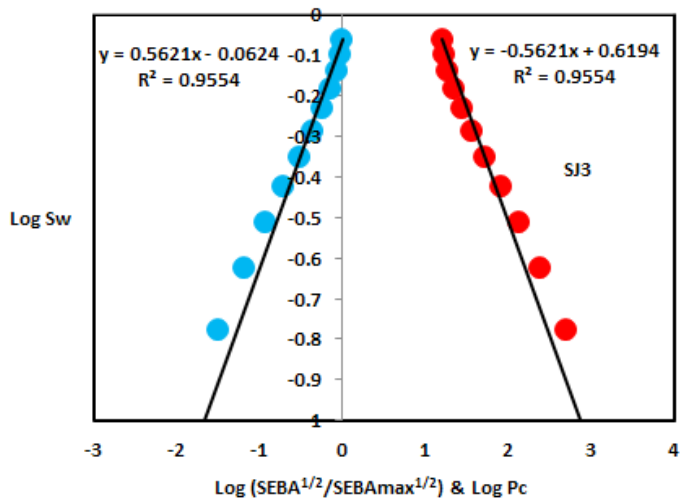

Figure 4: Log (SEBA$^{1/2}$ /SEBA$_{max}^{1/2}$) & log Pc versus log Sw for sample SJ3.

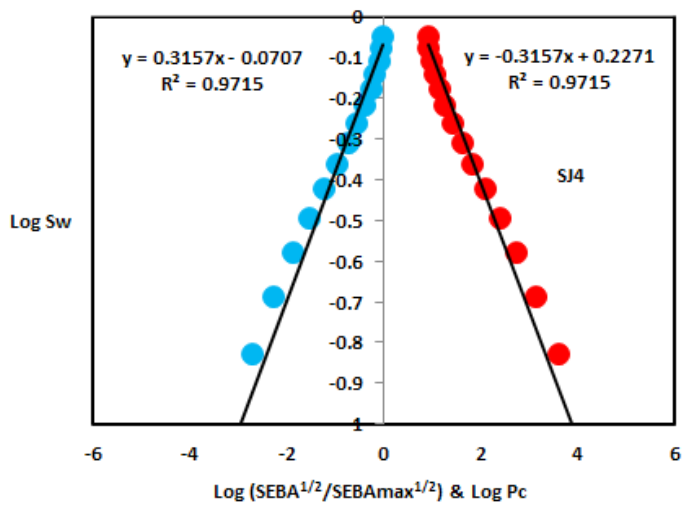

Figure 5: Log (SEBA$^{1/2}$ /SEBA$_{max}^{1/2}$) & log Pc versus log Sw for sample SJ4.

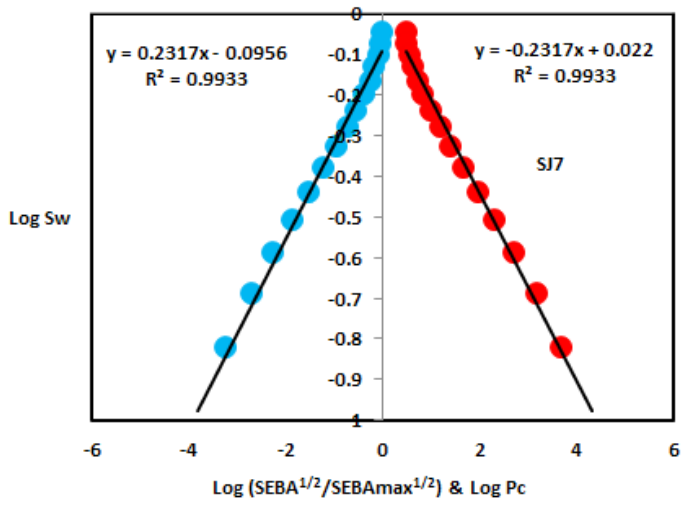

Figure 6: Log (SEBA$^{1/2}$/SEBA$_{max}^{1/2}$) & log Pc versus log Sw for sample SJ7.

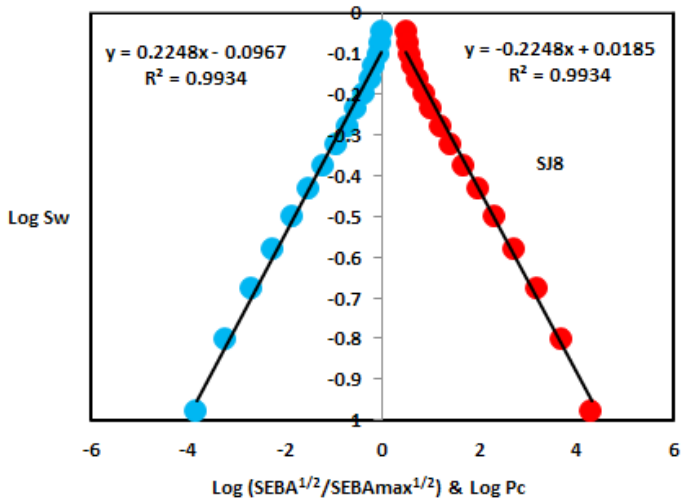

Figure 7: Log (SEBA$^{1/2}$/SEBA$_{max}^{1/2}$) & log Pc versus log Sw for sample SJ8.

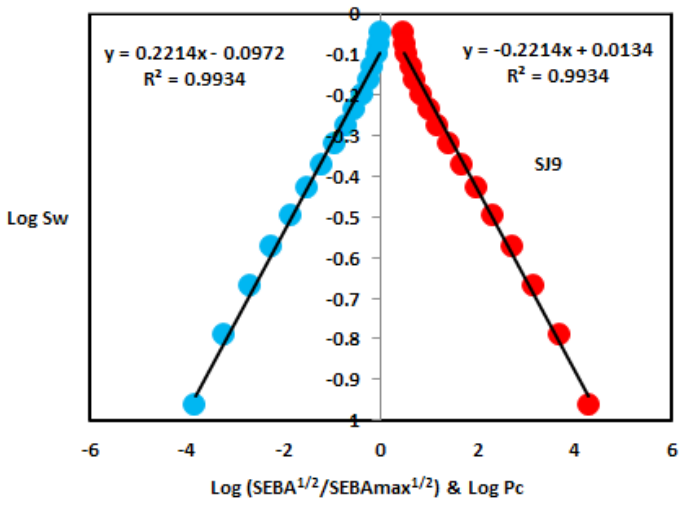

Figure 8: Log (SEBA$^{1/2}$/SEBA$_{max}^{1/2}$) & log Pc versus log Sw for sample SJ9.

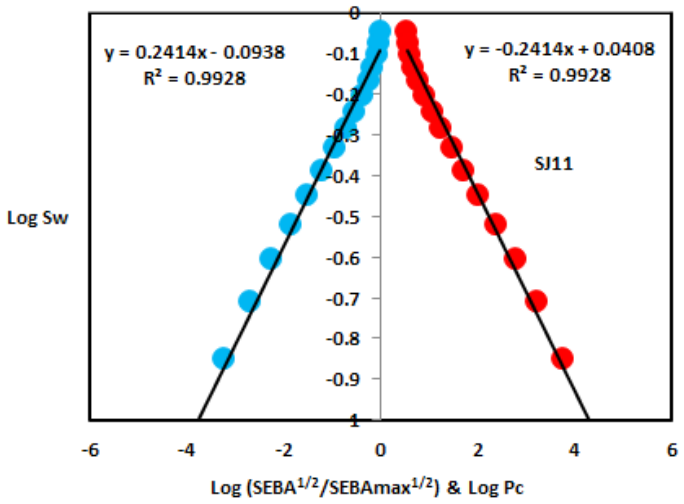

Figure 9: Log (SEBA$^{1/2}$/SEBA$_{max}^{1/2}$) & log Pc versus log Sw for sample SJ11.

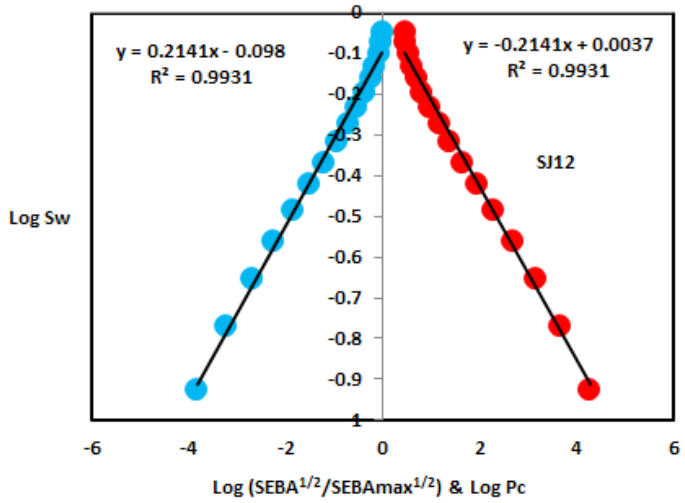

Figure 10: Log (SEBA$^{1/2}$/SEBA$_{max}^{1/2}$) & log Pc versus log Sw for sample SJ12.

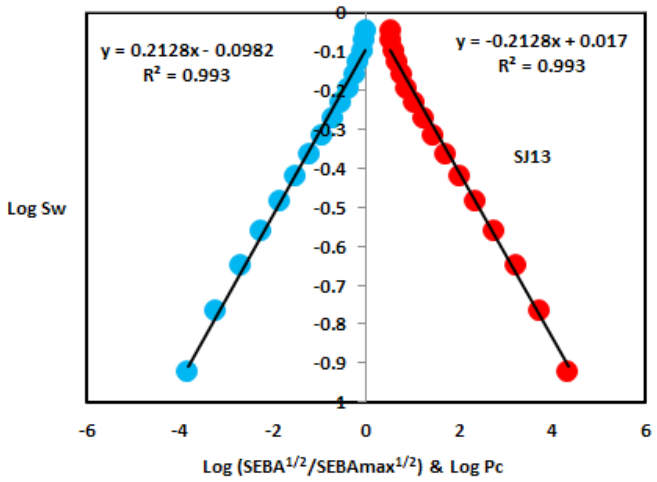

Figure 11: Log (SEBA$^{1/2}$/SEBA$_{max}^{1/2}$) & log Pc versus log Sw for sample SJ13.

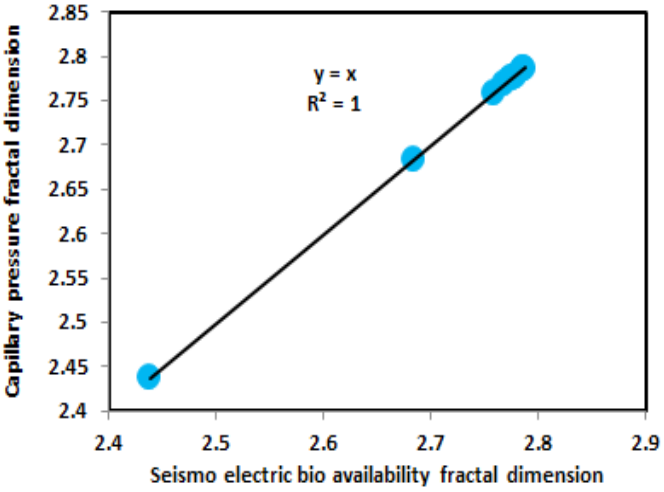

Figure12: Seismo electric bio availability fractal dimension versus capillary pressure fractal dimension.

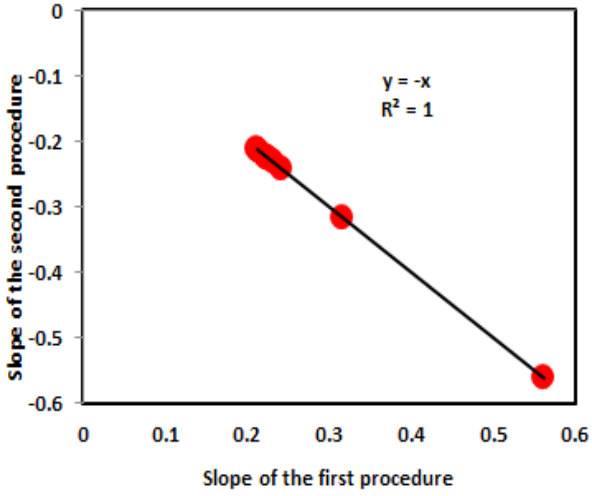

Figure 13: Slope of the first procedure versus slope of the second procedure.

Conclusion

The sandstones of the Shajara Reservoirs of the Permo-Carboniferous Shajara Formation were divided here into three units based on seismo electric bioavailability fractal. The Units from bottom to top are Lower Shajara seismo electric bio availability fractal dimension unit, Middle Shajara seismo electric bioavailability fractal dimension unit, and Upper Shajara seismo electric bio availability fractal dimension unit. These units were also confirmed by capillary pressure fractal dimension. The heterogeneity increases with increasing permeability, increasing fractal dimension, decreasing compaction owing to possibility of having interconnected channels.

Acknowledgement

The author would like to thank College of Engineering, King Saud University, Department of Petroleum and Natural Gas Engineering, Department of Chemical Engineering, Research Centre at College of Engineering and King Abdulla Institute for Research and Consulting Studies for their supports.

References

1. Frenkel J (1944) On the theory of seismic and seismoelectric phenomena in a moist soil. Journal of Physics 3: 230-241.
2. Li K, Williams W (2007) Determination of capillary pressure function from resistivity data. Transport in Porous Media 67: 1-15.
3. Revil A, Jardani A (2010) Seismoelectric response of heavy oil reservoirs: theory and numerical modelling. Geophysical Journal International 180: 781-797.
4. Dukhin AS, Goetz PJ, Thommes M (2010) Seismoelectric effect: a non-isochoric streaming current. 1 experiment. Journal of Colloid Interface Science, 345: 547-553.
5. Guan W, Hu H, Wang Z (2012) Permeability inversion from low-frequency seismoelectric logs in fluid-saturated porous formations. Geophysical Prospecting 61: 120-133.
6. Hu H, Guan W, Zhao W (2012) Theoretical studies of permeability inversion from seismoelectric logs. Geophysical Research Abstracts 14: 6725.
7. Bordes C, Sénéchal P, Barrière J, Brito D, Normandin E, Jougnot D, et al. (2015) Impact of water saturation on seismoelectric transfer functions: a laboratory study of co-seismic phenomenon. Geophysical Journal International 200: 1317-1335.
8. Jardani A, Revi A (2015) Seismoelectric couplings in a poroelastic material containing two immiscible fluid phases. Geophysical Journal International 202: 850-870.
9. Holzhauer J, Brito D, Bordes C, Brun Y, Guatarbes B (2017) Experimental quantification of the seismoelectric transfer function and its dependence on conductivity and saturation in loose sand. Geophysics Prospect 65: 1097-1120.
10. Rong P, Jian XW, Bang RD, Pin BD, Zi CL (2016) Experimental research on seismoelectric effects in sandstone. Applied Geophysics 13: 425-436.
11. Djuraev U, Jufar RS, Vasant P (2017) Numerical Study of frequency-dependent seismoelectric coupling in partially-saturated porous media. MATEC Web of Conferences 87: 02001.
12. Alkhidir KEME (2017) Pressure head fractal dimension for characterizing Shajara Reservoirs of the Shajara Formation of the Permo-Casrboniferous Unayzah Group, Saudi Arabia. Archives of Petroleum & Environmental Biotechnology 2: 1-7.
13. Alkhidir KEME (2018) Geometric relaxation time of induced polarization fractal dimension for characterizing Shajara Reservoirs of the Shajara Formation of the Permo-Carboniferous Unayzah Group, Saudi Arabia. Scifed Journal of Petroleum 2: 1-6.
14. Alkhidir KEME (2018) Geometric relaxation time of induced polarization fractal dimensionfor characterizing Shajara Reservoirs of the Shajara formation of the Permo-Carboniferous Unayzah Group-Permo. International Journal of Petrochemistry and Research 2: 1-6.
15. Alkhidir KEME (2018) Arithmetic relaxation time of induced polarization fractal dimension for characterizing Shajara Reservoirs of the Shajara Formation. Nanoscience and Nanotechnology 1: 1-8.